Chemically-invariant percolation in silver thioarsenate glasses and two ion-transport regimes over 5 orders of magnitude in Ag content

Rayan Zaiter, Mohammad Kassem, Daniele Fontanari, Maria Bokova, Fabrice Cousin, Takeshi Usuki, Eugene Bychkov

Chemically-Invariant Percolation in Silver Thioarsenate Glasses and Two Ion-Transport Regimes over 5 Orders of Magnitude in Ag Content

Rayan Zaiter [a], Mohammad Kassem [a,*], Daniele Fontanari [a], Maria Bokova [a], Fabrice Cousin [b], Takeshi Usuki [c], Eugene Bychkov [a,*]

[a] *Université du Littoral Côte d'Opale, 59140 Dunkerque, France*
[b] *Laboratoire Léon Brillouin, 91191 Gif sur Yvette, France*
[c] *Yamagata University, Yamagata 990-8560, Japan*

Abstract

Ionic conductivity σ_i measurements of AgY–As_2S_3 (Y = Br, I) glasses, covering 13 orders of magnitude in $\sigma_i(x)$ over 5 orders of magnitude in silver content x, confirm two drastically different ion transport regimes in silver halide thioarsenate glasses. As expected, the ionic conductivity in the critical percolation domain, 20 ppm < x ≤ 2 at.% Ag, follows a power-law dependence, $\sigma_i(x,T) \propto x^{T_0/T}$, where the critical temperature T_0 is related to the connectivity of the glassy host. Moreover, we show that $\sigma_i(x,T)$ is chemically invariant in the critical percolation domain. Three silver thioarsenate glass families, AgY- and Ag_2S-As_2S_3, reveal identical ionic conductivity within experimental uncertainty over three orders of magnitude in silver content x. The ionic conductivity diverges in the modifier-controlled region, x > 7-10 at.% Ag, and the difference in $\sigma_i(x)$ between AgI- and Ag_2S-As_2S_3 glasses approaches 4 orders of magnitude. Random distribution of silver in the critical percolation domain, shown by DFT modeling of neutron and high-energy x-ray diffraction data, is a key of the observed conductivity invariance. When silver cation leaves the residence site and travels throughout the glass network, characterized by the average Ag-Ag separation distance of 12 Å or more, the memory of its original chemical form (sulfide or halide) vanishes rapidly with increasing the mean square displacement. A non-random silver distribution in the modifier controlled region implying formation of preferential conduction pathways via direct contacts of edge- and corner-sharing silver chalcogenide or chalcohalide polyhedra rules out this possibility. Chemically-invariant ionic conductivity seems to be a common feature of any disordered system with random distribution of mobile ions having similar size of charge carriers.

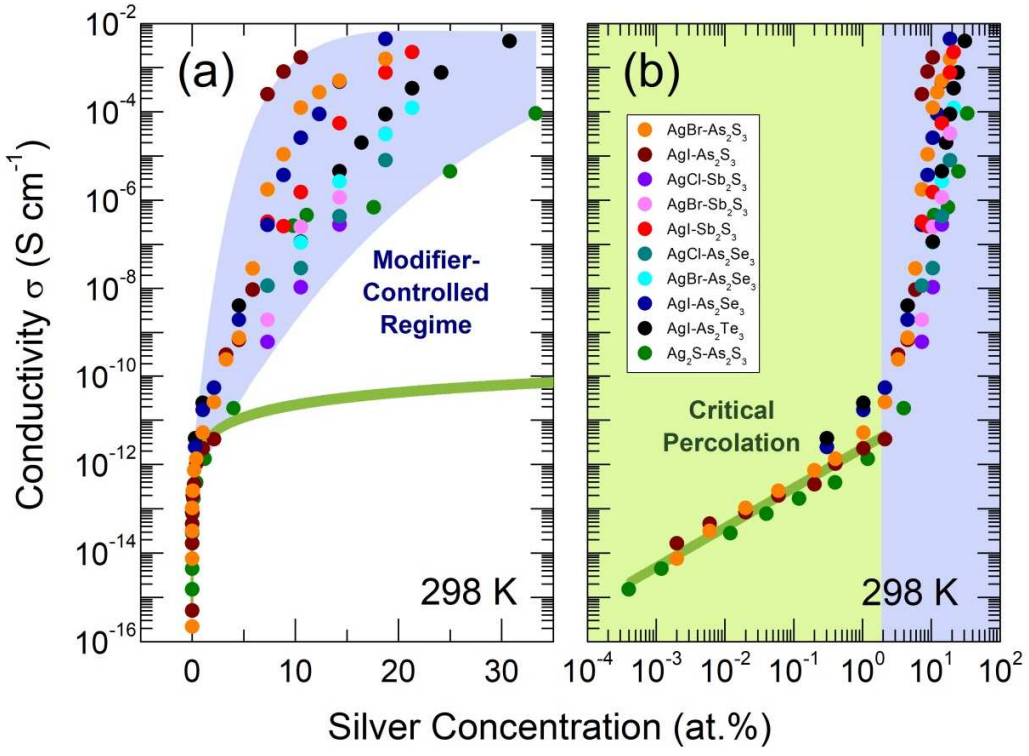

TOC Graphical Abstract

1. Introduction

Extensive studies of chalcogenide glass systems over the last decades resulted in their numerous applications in data and energy storage, optics and photonics, imaging and chemical sensing, see for example [1-5] and references therein. Vitreous chalcogenide alloys are also useful model systems to relate the glass composition and local structure at the short- and intermediate-range scale to various phenomena such as the glass transition and glass-forming ability, fast sub-nanosecond crystallization used in phase-change random access memory devices [6] and thermoelectric properties for future generations of solid-state refrigerators or thermoelectric generators [7]. All-solid-state lithium and sodium batteries, developed on the basis of superionic chalcogenide glass/ceramics [8,9], also need deeper understanding the relationships between composition, structure and ion transport properties for further optimization and improved performance. A vast majority of the published research in this field was focused on superionic chalcogenide materials with high mobile ion content. Much less attention was payed to cation-diluted glasses and to the origin of the ion transport in disordered solids.

One of the first reports dealing with conductivity studies over a wide composition range in mobile cation content was devoted to Na_2S-B_2S_3 glasses [10]. Nevertheless, the most studied systems appear to be silver sulfide and silver selenide vitreous alloys since they have excellent chemical stability and suitable ^{110m}Ag and ^{108m}Ag tracers for long-term diffusion experiments. Conductivity and tracer diffusion studies of silver and copper chalcogenide glasses over 3 to 5 orders of magnitude in Ag/Cu content [11-13] have shown two drastically different ion transport regimes above the percolation threshold at $x_c \approx 30$ ppm: (i) critical percolation, and (ii) modifier-controlled ion motion. The critical percolation transport was shown to be closely related to the connectivity of the glassy host reflected by the average coordination number $\langle n_0 \rangle$. The nature of mobile species (Ag^+ or Cu^+ cations), the chemical form of dopants (halides or chalcogenides) or of the host matrix (sulfide or selenide) appear to be much less important in a remarkable contrast to the modifier-controlled regime. However, the effect of the dopant chemical form has not been studied in details since the majority of the published results were related to selenide glassy systems [12-14] having the enhanced electronic conductivity, mostly of *p*-type, $\sigma_e > 10^{-12}$ S cm^{-1}, and masking the ionic transport at low cation content, $x < 0.3$ at.% or $100x_c$. The most extended mobile cation concentration range was studied in silver thioarsenate system Ag_2S-As_2S_3, from 4 ppm to 33.3 at.% Ag [15,16]. Vitreous arsenic sulfide host As_2S_3 has very low electronic conductivity, $\sigma_e \approx 2\times10^{-16}$ S cm^{-1} at room temperature [17], allowing the reliable ionic conductivity measurements of extremely diluted glasses to be compared with ^{110m}Ag tracer diffusion results [15,16]. We have chosen glassy As_2S_3 for silver halide AgY (Y = Br, I) doping to verify whether chemically different silver compounds will induce similar or contrasting Ag^+ ion transport in the critical percolation and modifier-controlled domains. We did not expect any surprises for glasses with high silver content since the widely accepted viewpoint predicts an increase of the ionic conductivity going from sulfide to halides: $\sigma_{Ag_2S-As_2S_3} < \sigma_{AgBr-As_2S_3} < \sigma_{AgI-As_2S_3}$. The open question was what happens for diluted or extremely diluted vitreous alloys.

2. Experimental

2.1. Glass Preparation

The $(AgBr)_y(As_2S_3)_{1-y}$, $0.0 \leq y \leq 0.6$, and $(AgI)_y(As_2S_3)_{1-y}$, $0.0 \leq y \leq 0.4$, glasses, were prepared from silver bromide and silver iodide respectively, with arsenic sulfide precursors via conventional high-temperature synthesis. The various components in the required proportion were sealed under vacuum (10^{-6} mbar) in silica tubes, heated up to 850 °C for 24 h before quenching in icy salt water. The AgY-poor glasses, $y < 0.01$, were prepared from more concentrated alloys using a dilution with the glassy host. Further synthesis details as well as basic glass characterization (XRD, DSC and density) will be published elsewhere.

2.2. Glass Homogeneity Measurements

Scanning electron microscopy, high-energy x-ray and pulsed neutron diffraction as well as small-angle neutron scattering experiments have been carried out to verify the amorphous state and homogeneity of selected glass samples. A JEOL JSM-7100F thermal field emission scanning electron microscope equipped with EDX Bruker QUANTAX 800 spectrometers was used to check the sample uniformity. Time-of-flight neutron diffraction experiments were carried out using GEM (ISIS Facility, UK) and GLAD (Argonne National Laboratory, USA) diffractometers. High-energy x-ray diffraction measurements were conducted at 6-ID-D beamline (Advanced Photon Source, USA) using 100 keV photons. The PAXY small-angle neutron scattering instrument (Laboratoire Léon Brillouin, France) was used for mesoscopic (10 to 1000 Å) structural studies using different neutron wavelengths and sample-to-detector distances: 5 Å/1.5 m, 5 Å/3.5 m, 8.5 Å/5 m, and 15 Å/6.7 m. Further experimental details are given in Supporting Information.

2.3. Conductivity Measurements

The *ac* electrical conductivity of the samples, σ_{ac}, was measured using a Hewlett Packard 4191A impedance meter. The impedance modulus Z and the phase angle θ were obtained in the frequency range 100 Hz to 15 MHz from room temperature up to 120 °C. The *dc* electrical conductivity of the samples, σ_{dc}, was measured using a Hewlett Packard 4339B high resistance meter using applied voltage of 100 volts. A maximum temperature for conductivity measurements was chosen to be below the glass transition temperature of the studied samples. The quenched glasses, prepared as rectangular plates, were polished using SiC powder with the grain size of 9.3 μ. The sample sides were ground parallel and gold was deposited on opposite sides to form electrodes for conductivity experiment. Typical thickness of the samples was in the range of 0.8–1.2 mm. The temperature dependence of conductivity was studied in several cycles, each consisting of a heating and a cooling step, in order to investigate a possible hysteresis.

3. Critical Percolation Regime in Ag^+ Ion-Conducting Glasses

Before description and discussion of the obtained experimental results, let us summarize state-of-the art of ion transport studies in chalcogenide glassy systems over a wide composition range in order to emphasize the established facts and open questions.

The ionic conductivity and tracer diffusion coefficient in the critical percolation domain, $x_c < x \leq 1$–3 at.% Ag, where $x_c \approx 30$ ppm Ag is the percolation threshold, follow a power-law composition dependence [11-13]

$$\sigma_i(x,T) = \sigma_i(1,T)x^{t(T)}, \quad (1)$$

$$D_{\mathrm{Ag}}(x,T) = D_{\mathrm{Ag}}(1,T)x^{t(T)-1}. \quad (2)$$

The temperature dependent power-law exponent $t(T)$ can be written as

$$t(T) = t_0 + T_0/T, \quad (3)$$

where $\sigma_i(1,T)$ and $D_{\mathrm{Ag}}(1,T)$ are the ionic conductivity and silver tracer diffusion coefficient, respectively, of a hypothetical percolation-controlled phase at the silver atomic fraction $x = 1$, t_0 is the critical exponent at $T = \infty$ and T_0 is the critical fictive temperature which reflects the interconnectivity of infinite percolation clusters. The conductivity or diffusion activation energy, $E(x)$, also depends on T_0

$$E(x) = E_0 - kT_0 \ln(x/x_c), \quad (4)$$

where E_0 is the activation energy at the percolation threshold x_c. In this regards, the second term of equation (4) portrays a configuration entropy term where $\ln(x/x_c)$ is related to the number and T_0 to the interconnectivity of conduction pathways frozen below glass transition temperature T_g. As such, the interconnectivity of clusters embedded in host matrix should depend on the host network connectivity if the dopant does not change significantly the microstructure organisation of the network.

A structural hypothesis [18] suggests the following simple pattern. (1) At $x < x_c$, the majority of silver ions reside in isolated domains. These domains are the allowed volumes of the glass [11,12] of 30 to 50 Å in diameter defined by local mean-square displacements of Ag^+ ions [19]. Consequently, the glass below x_c behaves as an electronic insulator. (2) In the critical percolation region above the percolation threshold, $x_c < x \leq \approx 1000x_c$, the previously isolated allowed volumes containing Ag^+ ions become connected forming infinite percolation clusters embedded in an insulating glassy host. The percolative ion transport depends on the number and interconnectivity of infinite percolation clusters. The latter is related to the connectivity of the host matrix reflected by the average coordination number

$$\langle n_0 \rangle = \sum_i x_i N_{ij}, \quad (5)$$

where x_i and N_{ij} are the atomic fraction and the local coordination number of species i in the glassy host. The average coordination number $\langle n_0 \rangle$ appears to be a key factor determining the critical

fictive temperature T_0, derived either from the conductivity and/or diffusion isotherms, Eqs. (1)-(3), or from the slope $\partial E(x)/\partial \ln x$, Eq. (4). A simple relationship was found between the critical fictive temperature T_0 and $\langle n_0 \rangle$,

$$T_0 \propto \langle n_0 \rangle - 2, \tag{6}$$

indicating that percolative transport is absent for chain structures, $T_0 = 0$ at $\langle n_0 \rangle = 2$, which is identical to the classical models [20,21] stating the absence of percolation for 1D networks.

The Haven ratio H_R is an important parameter, reflecting correlation effects in ionic motion and defined as [22]

$$H_R = \frac{D^*}{D_{\sigma_i}}, \tag{7}$$

where D^* is the tracer diffusion coefficient and D_{σ_i} the conductivity diffusion coefficient, calculated from the ionic conductivity σ_i using the Nernst-Einstein relation

$$D_{\sigma_i} = \frac{kT\sigma_i}{x(ze)^2}, \tag{8}$$

where ze is the charge of the mobile cation and x its concentration.

The Haven ratio in the critical percolation regime decreases monotonically with increasing x or decreasing the Ag-Ag interatomic separation distance $r_{\mathrm{Ag-Ag}}$ [11-13]

$$H_R = 1 - \frac{const}{r_{\mathrm{Ag-Ag}}}. \tag{9}$$

The observed change from uncorrelated ionic migration, $H_R = 1$ in the Ag dilution limit: $r_{\mathrm{Ag-Ag}} \rightarrow \infty$, to a correlated ionic motion ($H_R \approx 0.5$) suggests a random distribution of mobile cations when the Ag-Ag separation distance is a hyperbolic function of x

$$r_{\mathrm{Ag-Ag}} = 2\left(\frac{3}{4\pi}\frac{V_a}{N_A x}\right)^{1/3}, \tag{10}$$

where V_a is the mean atomic volume and N_A the Avogadro's number. Interionic interactions of Ag^+ cations, increasing with decreasing $r_{\mathrm{Ag-Ag}}$, led to correlation effects in the ionic diffusion.

It was also suggested that neither the nature of mobile cations (Ag^+ or Cu^+) nor the dopant chemical form (metal halide or chalcogenide) plays any important role in the critical percolation, as well as the chemical form of the host matrix. This hypothesis has not been checked in details since the majority of the studied glasses in the critical percolation domain having identical average coordination of the glassy host, $\langle n_0 \rangle = 2.40$, belong to selenide systems: AgI-As_2Se_3, CuI-As_2Se_3, Cu_2Se-As_2Se_3 [12-14]. The only exception was the silver thioarsenate family, Ag_2S-As_2S_3 [15-16]. Enhanced *p*-type electronic conductivity of selenide glasses [17] is masking the ionic contribution at low x. A complete set of tracer diffusion measurements was also hardly to be realized since the short half-life of the ^{64}Cu tracer ($t_{½}$ = 12.7 hours) restricts seriously the duration of diffusion

anneals and the accessible diffusion coefficients. The best solution to verify the conductivity invariance in the critical percolation domain is to work with silver halide thioarsenate systems AgY-As_2S_3 (Y = Br, I).

4. Results and Discussion

4.1. Glass Homogeneity

The two silver halide thioarsenate $(AgY)_y(As_2S_3)_{1-y}$ families reveal quite extended glass-forming regions: $y_{max} \leq 0.6$ for the AgBr-glasses and $y_{max} \leq 0.4$ for their AgI-counterparts. Glasses at the limit of the glass-forming range exhibit Bragg peaks corresponding to crystalline silver halides when synthesized in large quantity (≈10 g), Fig. 1(b). Smaller samples (0.3-3 g) either do not show the Bragg peaks or their intensity becomes negligible, Fig. 1(a).

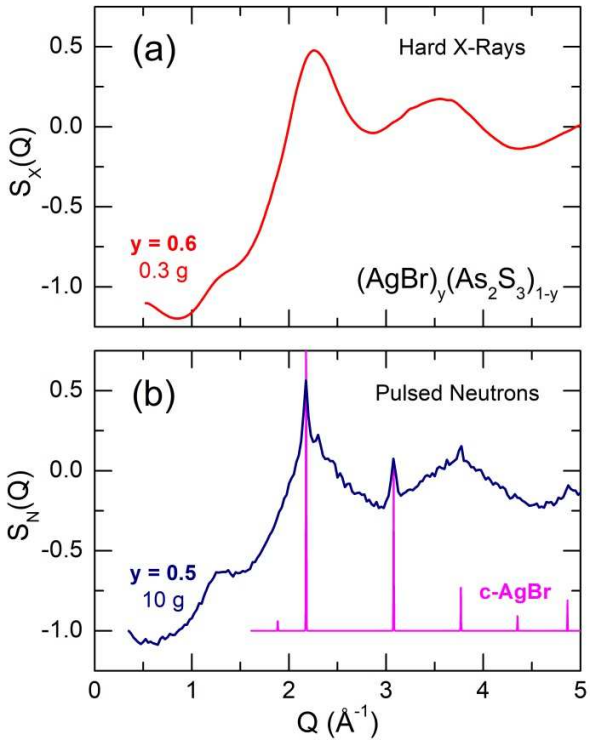

Fig. 1. A low-Q part of (a) the x-ray $S_X(Q)$ and (b) neutron $S_N(Q)$ structure factors for AgBr-rich thioarsenate glasses. A small y = 0.6 glass sample (0.3 g) was used for high-energy x-ray diffraction experiments. A much larger y = 0.5 sample (10 g) was measured using pulsed neutrons. Characteristic Bragg peaks of cubic AgBr, space group $Fm\bar{3}m$ [23] are also shown.

Silver thioarsenate glasses Ag_2S-As_2S_3 appear to be phase-separated within the intermediate silver concentration range, $4 \leq x \leq 18$ at.% Ag, forming silver-rich and Ag-poor vitreous domains [24,25]. Consequently, we have checked the homogeneity of $(AgY)_y(As_2S_3)_{1-y}$ glasses on mesoscopic level. Preliminary scanning electron microscopy (SEM) and small-angle neutron scattering (SANS) studies show that silver-poor glasses ($y \leq 0.2$, $x \leq 4$ at. % Ag) are homogeneous, while at

intermediate silver concentrations (x > 4 at.% Ag), a mesoscopic phase separation was observed, Figs. 2 and 3.

The SEM images of two AgBr-As_2S_3 glasses are shown in Fig. 2. The y = 0.2 sample appears to be uniform, while the y = 0.3 glass specimen exhibits multiple spherical objects of typical size between 50 and 300 nm. The latter backscattered electron image contains also chemical information; brighter spherical particles are enriched with silver compared to darker glass matrix, confirmed also by energy dispersive x-ray (EDX) analysis.

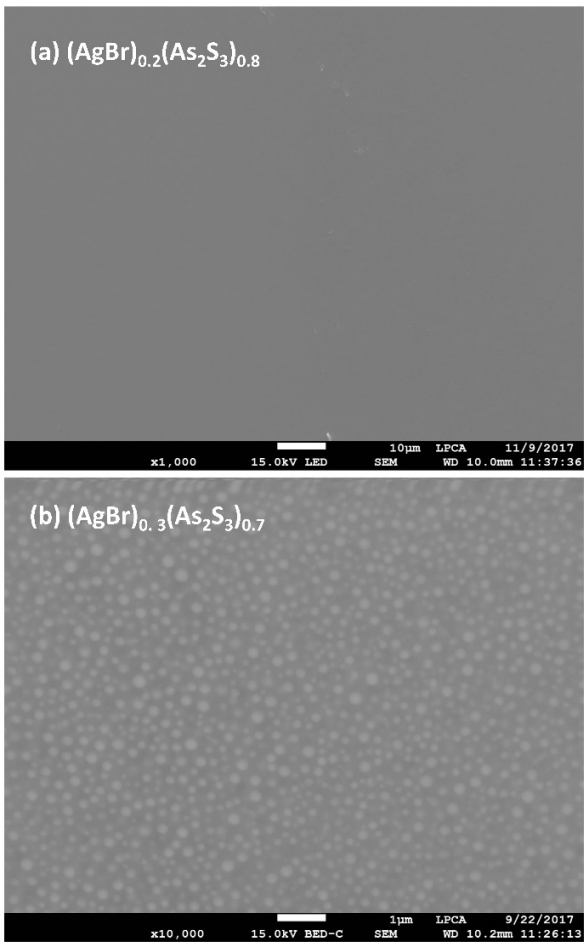

Fig. 2. Scanning electron microscopy images of $(AgBr)_y(As_2S_3)_{1-y}$ glasses: (a) y = 0.2, (b) y = 0.3. The secondary electron detection was used for the y = 0.2 sample. The backscattered electron image was taken for the y = 0.3 glass.

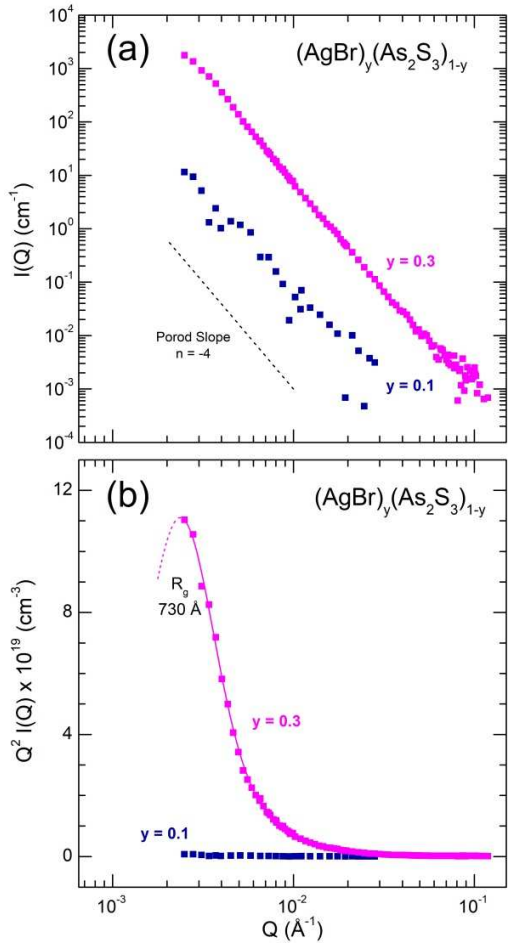

Fig. 3. Small-angle neutron scattering data for $(AgBr)_y(As_2S_3)_{1-y}$ glasses: (■, blue) y = 0.1, and (■, magenta) y = 0.3; (a) the normalized SANS intensity $I(Q)$ plotted on a log-log scale; (b) the Kratky plot: $Q^2\,I(Q)$ vs. Q. The Porod slope n = -4 is also shown.

The SEM observations appear to be coherent with small-angle neutron scattering experiments, Fig. 3. The normalized SANS intensity $I(Q)$ of two AgBr-As_2S_3 glass samples plotted on a log-log scale shows a remarkable difference of two orders of magnitude between the y = 0.1 and y = 0.3 glasses. The both scattering functions roughly follow a Porod law $I(Q) \propto Q^{-4}$ [26,27]. Nevertheless, the

slope $n = \partial \log I(Q)/\partial \log Q$ = -3.5±0.1 is lower for the Ag-poor glass. Moreover, the $I(Q)$ shape and magnitude for the y = 0.1 sample are typical for homogeneous chalcogenide glasses with density fluctuations and rather well described by the Debye-Bueche model [28] with a characteristic correlation distance of ≈200 Å [24,29,30]. Much more intense $I(Q)$ for the y = 0.3 sample exhibits some positive deviations from the Porod slope n = -4 below 5×10^{-3} Å^{-1} with a subsequent slope decrease. However, the accessible Q-range ($Q_{min} \approx 2 \times 10^{-3}$ Å^{-1}) does not allow to follow further evolution, presumably a Guinier regime [26,27], n = -2, at lower Q. The Kratky plot, $Q^2\, I(Q)$ vs. Q, Fig. 3(b), is often used to estimate a typical size of mesoscopic particles if the Guinier approximation is valid [31]. In this case, the function $Q^2\, I(Q)$ plotted versus the scattering vector Q shows a maximum. The position of this maximum, Q_{max}, and the Guinier radius of gyration R_g are related, $Q_{max} = \sqrt{3}/R_g$. Here again, the limited Q-range does not allow to observe a clear maximum. Nevertheless, a rough estimation of R_g = 730±200 Å is consistent with the SEM data.

Resuming, we conclude that silver-poor AgBr-As_2S_3 glasses, $y \leq 0.2$, are homogeneous at mesoscopic scale showing only density fluctuations while the glasses with silver content, $y > 0.2$, are phase-separated and exhibit Ag-enriched spherical mesoscopic regions of approximate size 50 to 300 nm. For theAgI-As_2S_3 system, the glass compositions with $y \leq 0.15$ are homogeneous while the silver rich composition (y = 0.4) is not as indicated the non-unique glass transition temperature of the DSC curve, Fig. S2 (supporting information).

The origin of phase separation in glasses is often a philosophical question and hard to answer. Considering that the structural motifs in homogeneous silver glasses are related to their crystalline counterparts, one can give the hypothesis that the absence of Ag-poor crystals (= their thermodynamic instability), for a certain system, explains a wide composition range of phase-separated glasses consisting of silver-poor and silver-rich glassy phases. This is confirmed by SEM images of AgBr-As_2S_3 glasses, $0.0 \leq y \leq 0.6$, presented in supporting information (Figure S1). Regarding the phase-separated composition with y = 0.3, the Ag-poor phase is the dominant and the Ag-rich phase appears in the form of spherical droplets. For higher Ag concentrations, in particular for y = 0.5, the situation changes drastically and the Ag-rich phase becomes the dominant one. The larger Ag-rich domains, interestingly contain inclusions of Ag-poor phase of various sizes. In particular, when the Ag concentration exceeds ~7 at.% ($y > 0.3$) the initially continuous Ag-poor phase becomes fragmented and the Ag-rich phase percolates in the glass structure. The size of the Ag-poor droplets also spans a wide range in spatial scale. Increasing further the Ag content, with y = 0.6 causes the disintegration of the sizeable Ag-poor droplets to much smaller ones and the reduction of the size polydispersity; sizes of the Ag-poor droplets do not exceed 2–3 μm. Interestingly, it is at $y > 0.3$ that an abrupt change of ionic conductivity is seen for the AgBr-As_2S_3 glasses, related to the formation of a continuous Ag-rich phase in the phase-separated glasses, Fig. 5(a).

4.2. Electric Transport

Typical conductivity temperature dependences for the AgY-As_2S_3 glasses are shown in Fig. 4.

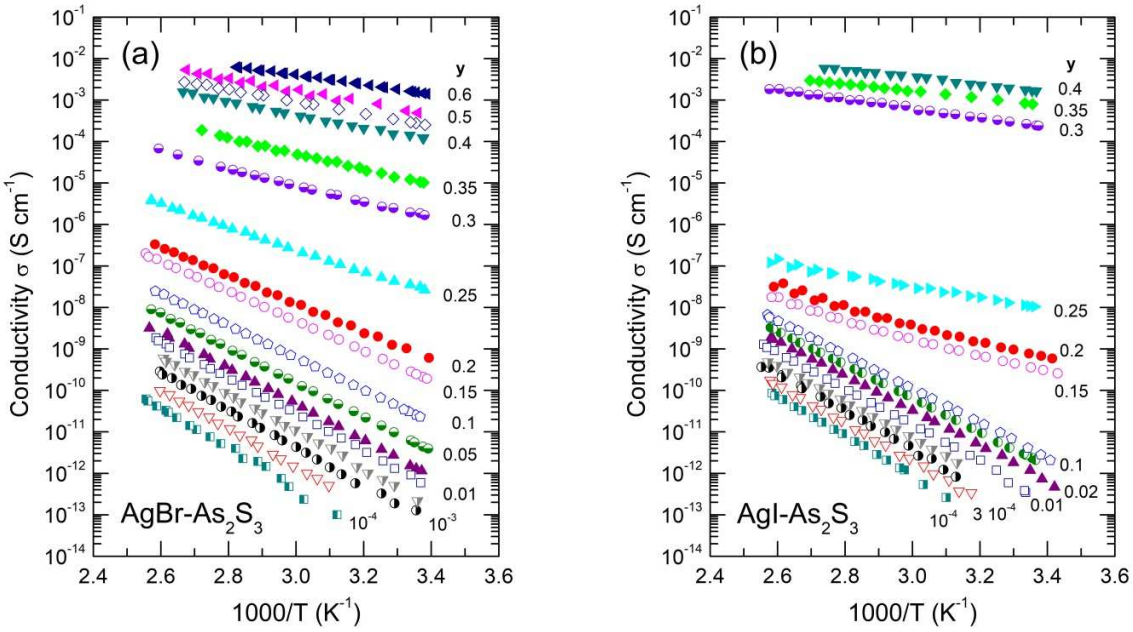

Fig. 4. Temperature dependences of the total electrical conductivity σ for the (a) $(AgBr)_y(As_2S_3)_{1-y}$ and (b) $(AgI)_y(As_2S_3)_{1-y}$ glass systems. The numbers for selected glasses indicate the AgY molar fraction y.

The electrical conductivity, determined either by the complex impedance method ($\sigma \geq 10^{-8}$ S cm^{-1}) or from the *dc* conductivity measurements ($\sigma < 10^{-8}$ S cm^{-1}), does not show any significant hysteresis and obeys the Arrhenius law

$$\sigma = \frac{\sigma_0}{T} \exp\left(-\frac{E_a}{kT}\right), \tag{11}$$

where σ_0 is the conductivity pre-exponential factor, E_a the activation energy, k the Boltzmann constant and T the temperature. The room temperature conductivity σ_{298}, σ_0 and E_a were calculated from a least-square fit of the data to Eq. (11). The results are summarized in Tables S1 and S2 (Supporting Information) and shown in Figs. 5 and 6.

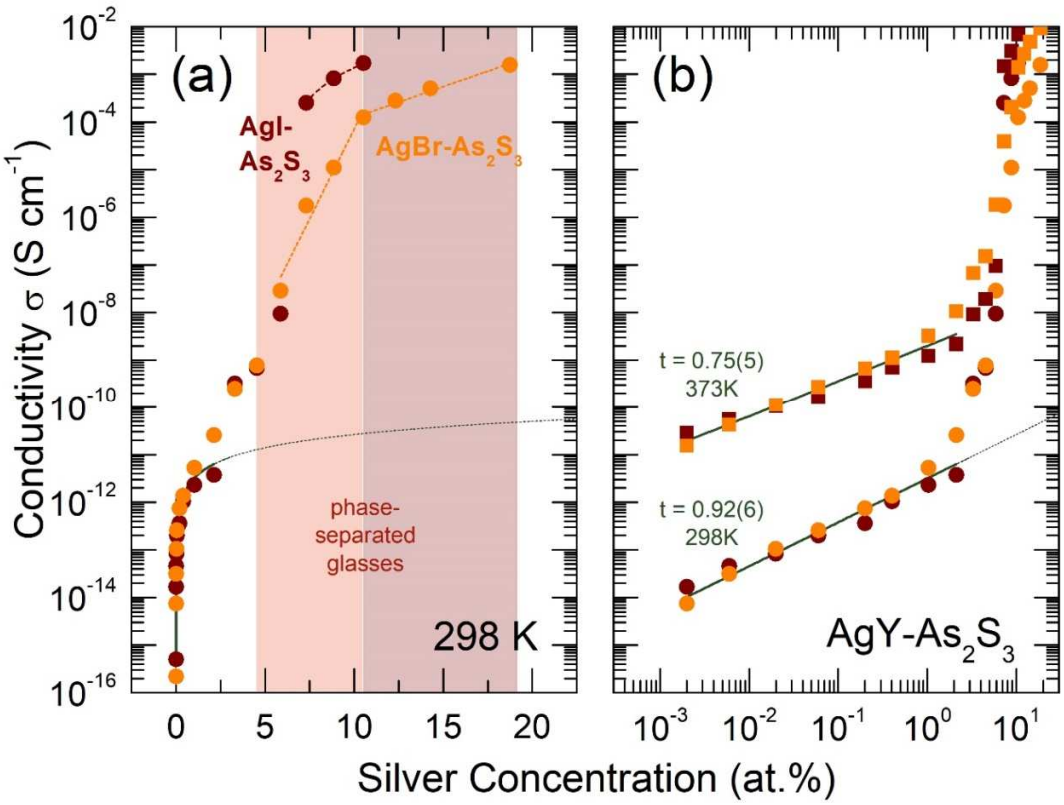

Fig. 5. (a) Room-temperature conductivity of (●, orange) AgBr-As_2S_3 and (●, brown) AgI-As_2S_3 glasses plotted on a semi-logarithmic scale, and (b) the conductivity isotherms of silver halide thioarsenate glasses at (●●, solid circles) 298 K and (■■, solid squares) 373 K plotted on a log-log scale. The solid lines represent a least-square fit of the experimental data points in the critical percolation domain to Eq. (1); the thin short dashed lines show hypothetical conductivity data beyond the percolation domain; the bold dashed lines in the modifier-controlled domain are drawn as a guide to the eye. An approximate composition range of phase-separated glasses is highlighted in red.

The room-temperature conductivity (Fig. 5) increases by ≈13 orders of magnitude with increasing silver halide content from the values which are typical for insulating sulfide glasses (10^{-16} S cm^{-1}) [17] to the values which are characteristic of superionic vitreous alloys (10^{-3} S cm^{-1}) [8,9]. The maximum room-temperature conductivity is 1.6 × 10^{-3} S cm^{-1} for the AgBr-rich glasses (y = 0.6, x = 18.75 at.% Ag) and 1.7 × 10^{-3} S cm^{-1} for the AgI-rich alloys containing 10.53 at.% Ag (y = 0.4). This enormous change in conductivity is accompanied by a drastic decrease of the activation energy from 1.0 to 0.2 eV, Fig. 6(a). In contrast, the pre-exponential factor σ_0 in both systems remains rather invariant up to 4 at.% Ag (AgBr-As_2S_3) or 2 at.% Ag (AgI-As_2S_3), $\sigma_0 \approx 2 \times 10^5$ S cm^{-1} K, and then drops to ≈2 × 10^4 S cm^{-1} K for AgBr-rich glasses or to ≈10^3 S cm^{-1} K for their silver iodide counterparts, Fig. 6(b). We should also note that glasses in the AgI-As_2S_3 system, 0.15 ≤ y ≤ 0.25, are characterized by unusually low values of σ_0 = 1 – 10 S cm^{-1} K. In addition, the phase-separated glasses in the two systems show non-monotonic changes at intermediate silver concentrations, 4 ≤ x ≤ 10 at.% Ag, both in σ_{298} and E_a, Figs. 5 and 6. Figures 4-6 clearly show two drastically different composition trends in conductivity parameters: (i) the critical percolation below 2 at.% Ag, and (ii)

the modifier-controlled regime at higher silver content, x > 7-10 at.% Ag. The exact starting concentration of the modifier-controlled region is difficult to establish because of phase-separation.

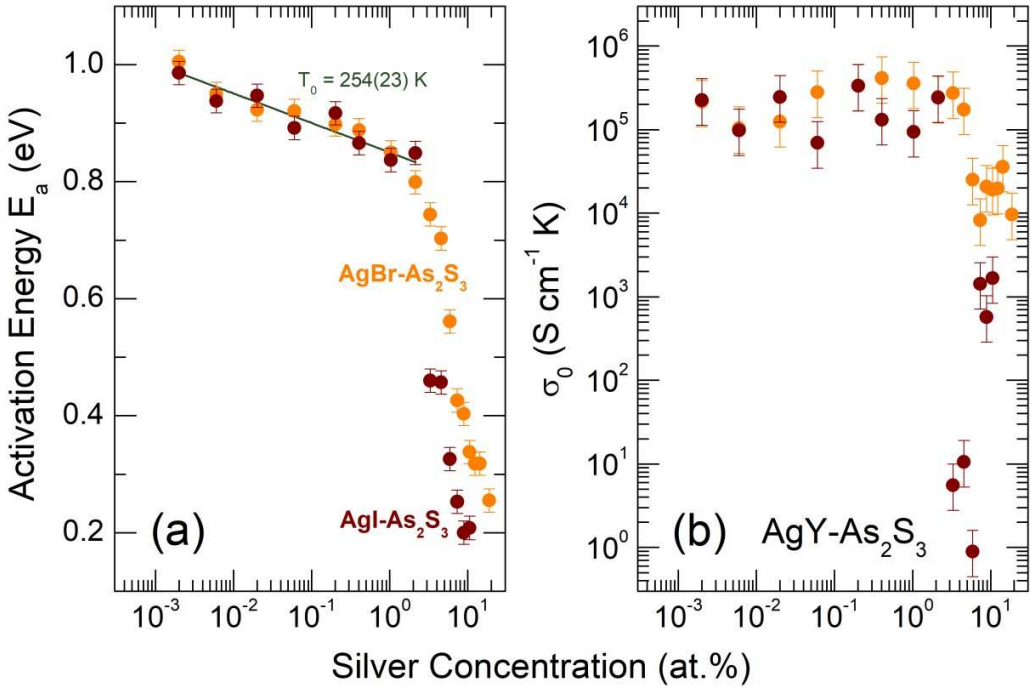

Fig. 6. (a) Conductivity activation energy E_a and (b) conductivity pre-exponential factor σ_0 of (●, orange) AgBr-As_2S_3 and (●, brown) AgI-As_2S_3 glasses. The solid line represents a least-square fit of the E_a experimental data points in the critical percolation domain to Eq. (4).

4.2.1. Critical percolation domain, 20 ppm < x ≤ 2 at.% Ag

The conductivity isotherms of AgY-As_2S_3 glasses at 298 and 373 K are consistent with the expected critical percolation behavior, revealing the power-law composition dependences, Eq. (1), over 3 orders of magnitude in silver content x and two orders of magnitude in σ, Fig. 5(b). The critical exponent $t(T)$ decreases with increasing temperature in accordance with Eq. (3): t(298K) = 0.92±0.06 and t(373K) = 0.75±0.05. The conductivity activation energy follows Eq. (4) and shows a linear decrease of $E_a(x)$ on a logarithmic concentration scale, Fig. 6(a). However, the most important and new result of the conductivity study is a *chemically-invariant* critical percolation since the conductivity parameters of AgY-As_2S_3 (this work) and Ag_2S-As_2S_3 (Ref. 15) glasses appear to be identical within experimental uncertainty. The maximum conductivity difference between the three systems does not exceed ±0.3 log σ_i units. The conductivity invariance indicates also that the measured electrical conductivity in the AgY-As_2S_3 glasses is essentially ionic as it was verified for the Ag_2S-As_2S_3 system using ^{110m}Ag tracer [16]. Nevertheless, we are planning silver tracer diffusion measurements to validate this conclusion and to study correlation effects of the ion transport.

Figure 7 shows the average values of the critical exponent $t(T)$ calculated for these three thioarsenate families and plotted as a function of reciprocal temperature. A perfect fit of the

experimental data points to Eq. (3) is observed with $t_0 \cong 0$ as for other chalcogenide systems [11-14]. The derived average critical temperature T_0 = 264±4 K appears to be very similar to that calculated from $E_a(x)$ using Eq. (4), T_0 = 254±23 K. The individual critical temperatures for each thioarsenate as well as selenoarsenate family with $\langle n_0 \rangle$ = 2.40 are mutually consistent with these average values and follow the host connectivity, Eq. (6), Fig. 8.

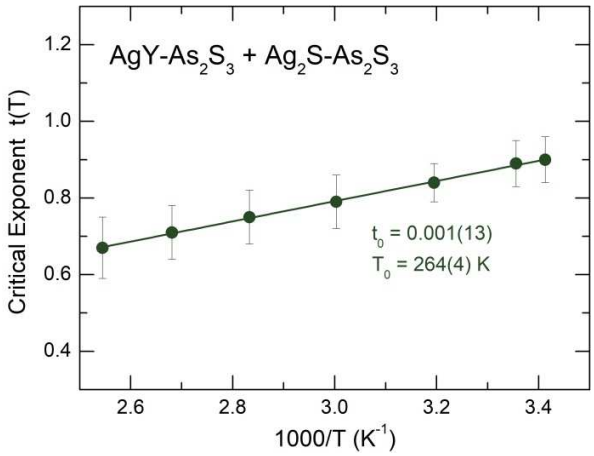

Fig. 7. Average values of the critical exponent $t(T)$ calculated for AgY- and Ag_2S-As_2S_3 glasses at $x \leq 2$ at.% Ag and plotted as a function of reciprocal temperature. The derived t_0 and T_0 parameters are also shown.

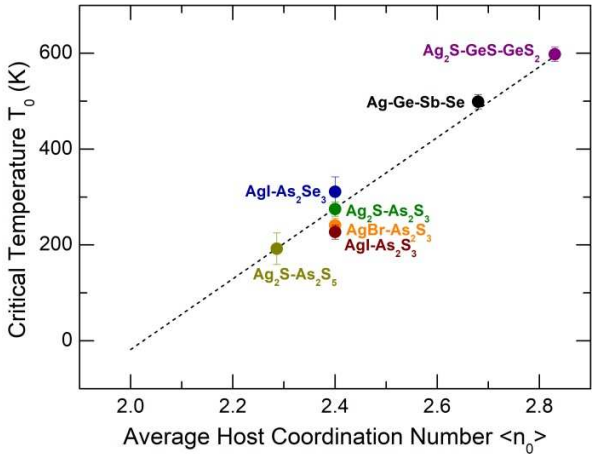

Fig. 8. Critical fictive temperature T_0 plotted as a function of the average local coordination number $\langle n_0 \rangle$ of the host matrix for a number of chalcogenide and chalcohalide glasses. All data points, except for AgY-As_2S_3 (this work), were taken from ref. 13.

4.2.2. Modifier-controlled region, x > 7-10 at.% Ag

The ionic conductivity diverges from chemically-invariant behavior in the modifier-controlled domain at higher x. Figure 9 shows the room-temperature conductivity isotherms of the investigated silver halide thioarsenate glasses and their selenoarsenate AgY-As_2Se_3, telluroarsenate AgI-As_2Te_3 and thioantimonate AgY-Sb_2S_3 counterparts [13,32-35], as well as of Ag_2S-As_2S_3 vitreous alloys [15,16]. Most of the data were only obtained in the modifier-controlled domain because of enhanced electronic conductivity of selenide and especially telluride glasses. In the AgI-As_2Te_3 system, we have used the ion transport numbers t_{Ag^+}, obtained from a combined conductivity and ^{108m}Ag tracer diffusion study [34], to calculate the ionic conductivity up to 0.3 at.% Ag.

As expected, the modifier-controlled ionic conductivity varies strongly when changing the chemical form of silver reaching 4 orders of magnitude between $\sigma_{Ag_2S-As_2S_3}(x)$ and $\sigma_{AgI-As_2S_3}(x)$. The nature of halide species also appears to be important; substitution of AgCl by AgBr increases the ionic conductivity by a factor of 4 to 30. The AgBr/AgI change is accompanied by further increase in σ_i, $40 \leq \sigma_{AgI-host}(x)/\sigma_{AgBr-host}(x) \leq 200$. A clear effect is observed changing the chalcogen: $\sigma_{AgI-As_2S_3}(x) > \sigma_{AgI-As_2Se_3}(x) > \sigma_{AgI-As_2Te_3}$. Vitreous silver halide thioantimonates are also less conducting than their thioarsenate counterparts.

The ionic conductivity increases exponentially at intermediate silver concentrations

$$\sigma_i(x) \propto \exp(ax), \tag{12}$$

where a is a constant. Nevertheless, one observes a saturation trend at higher x, and the room-temperature ionic conductivity seems to be limited by $\sigma_{298} \approx 10^{-2}$ S cm^{-1}. This or similar conductivity level was reached at $x \approx 10$ at.% Ag for AgI-As_2S_3, $x \approx 20$ at.% Ag for AgI-As_2Se_3, and $x \approx 30$ at.% Ag for AgI-As_2Te_3 glasses. We should also note an enhanced electronic conductivity in selenide and especially telluride AgI-As_2Te_3 glasses, which are predominantly electronic conductors at $x < 0.5$ [34]. The Te 5p lone pair electron states, situated in the top of the valence band, are decreasing the bandgap and increasing the electronic conductivity. Silver tracer diffusion measurements also show that ionic conductivity in telluride systems is by a factor of 100 lower than in sulfide and selenide counterparts [34,36]. This difference seems to be caused by a higher glass packing density of the telluride network. In particular, the fraction of microscopic voids and cavities in glassy As_2S_3 is 44% of the total glass volume [37] while in g-As_2Te_3 it is only 14% [38].

The phase-separated glasses exhibit a non-monotonic behavior at intermediate concentrations. The homogenous vitreous alloys, i.e., AgI-As_2Se_3 or AgI-As_2Te_3, reveal smooth conductivity isotherms [32,34].

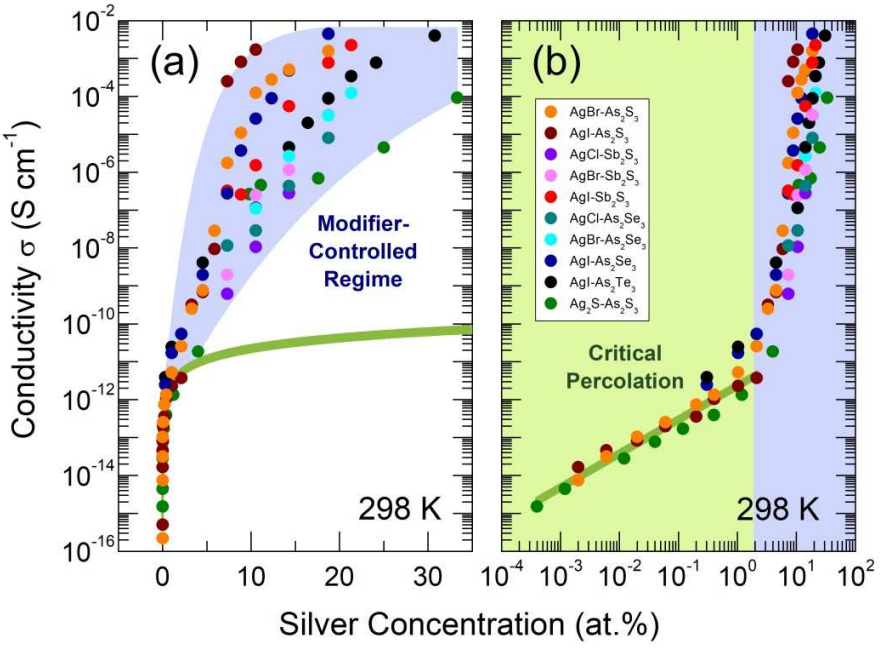

Fig. 9. Room-temperature ionic conductivity isotherms of AgY-As_2S_3 (Y = Br, I) (this work), AgY-As_2X_3 (Y = Cl, Br, I; X = Se, Te) [32-34], AgY-Sb_2S_3 (Y = Cl, Br, I) [35] and Ag_2S-As_2S_3 glasses [15-16]; (a) a linear concentration scale, (b) a log-log plot. The bold green solid line shows chemically-invariant power-law composition dependence of $\sigma_{298}(x)$, Eq. (1), for three families of silver thioarsenate glasses in the critical percolation domain. The modifier-controlled region is highlighted in light blue.

4.3. Structural Differences between Critical Percolation and Modifier-Controlled Domains

The contrasting composition dependences of ionic conductivity in the critical percolation and modifier-controlled domains suggest structural differences between diluted and Ag-rich glasses. A random distribution of silver species at $x \leq 2$ at.% Ag looks reasonable, confirmed by small-angle neutron scattering of homogeneous Ag_2S-As_2S_3 glasses belonging to the both regions [24]. A common mesoscopic feature of the two glass series was density fluctuations with a characteristic Debye-Bueche correlation distance of 160±15 Å, similar to those observed for the $(AgBr)_{0.1}(As_2S_3)_{0.9}$ sample, Fig. 3. However, the Ag-related difference scattering functions [39], $\Delta I_{Ag}(Q)/\sum_i (x_i \bar{b}_i)^2$, appear to be different for Ag-poor and Ag-rich glasses, reflecting homogeneous silver distribution in the critical percolation domain and some Ag clustering in the modifier-controlled region [24]. A non-random silver distribution in Ag-rich glasses was observed in numerous diffraction studies of silver chalcogenide glasses, revealed by short Ag-Ag correlations at 3 Å [12,40-43]. This characteristic Ag-Ag separation appears to be shorter than that calculated assuming a random silver distribution, e.g. using a Wigner-Seitz type equation (10). Consequently, some local glass zones have higher silver content than the other, giving rise to a modified glass network [44], widely used for description of cation-rich vitreous alloys [45-49].

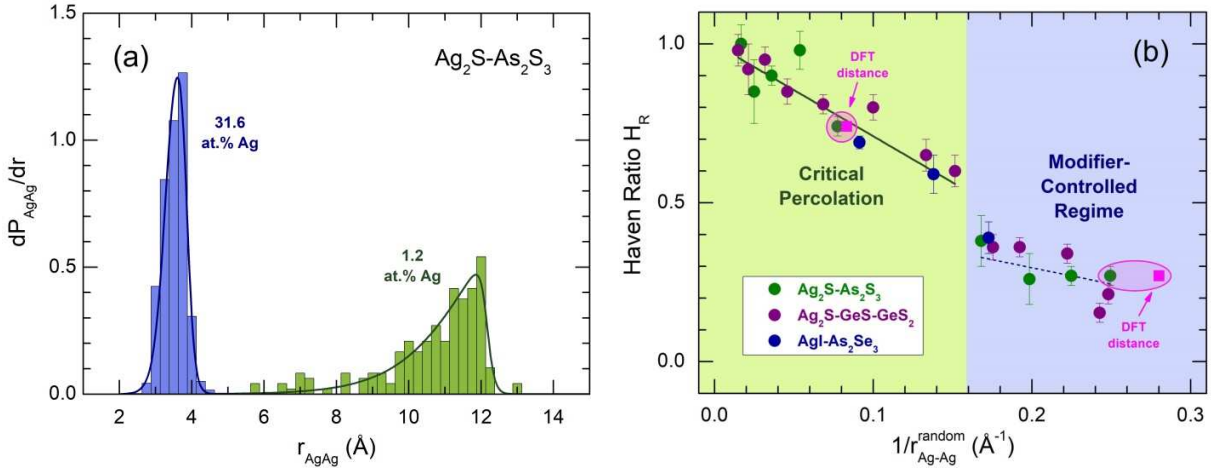

Fig. 10. (a) Connectivity analysis of Ag-Ag distributions in the x = 1.2 at.% Ag (critical percolation region) and x = 31.6 at.% Ag (modifier-controlled domain) glasses. The analyzed DFT data correspond to the average values of 10 simulation boxes containing either 988 (x = 1.2 at.% Ag) or 1007 (x = 31.6 at.% Ag) silver, arsenic and sulfur atoms. (b) The Haven ratio H_R in Ag_2S-As_2S_3, Ag_2S-GeS-GeS_2, and AgI-As_2Se_3 glasses [11,12,16] plotted as a function of reciprocal Ag-Ag distance, calculated assuming a random distribution of silver. The solid magenta squares show the H_R for the x = 1.2 and 31.6 at.% Ag glasses plotted using the derived Ag-Ag distances from DFT modelling. The solid line in Fig. 10(b) represents the result of a least-square fit of the experimental data points to Eq. (9). All other lines are drawn as a guide to the eye.

We have used a DFT structural modelling of two Ag_2S-As_2S_3 glasses to obtain quantitative estimations of Ag-Ag separation distances in the critical percolation domain (x = 1.2 at.% Ag), which are missing in all published reports, and modifier-controlled region (x = 31.6 at.% Ag). Figure 10(a) shows a connectivity analysis of DFT simulation boxes for the two glasses. The derivative of the bound silver fraction, $\partial P_{AgAg}(r)/\partial r$, for the 1.2 at.% Ag glass is centered at ≈12 Å,

indicating that the average derived Ag-Ag separation appears to be nearly identical to that calculated for a random silver distribution. We note that the bound silver fraction $P_{\mathrm{AgAg}}(r)$ is defined as a fraction of silver species having at least one nearest or distant neighbor at the distance *r*. In contrast, a $\partial P_{\mathrm{AgAg}}(r)/\partial r$ maximum for the 31.6 at.% Ag glass arises at shorter distances than expected for random distribution, in accordance with the reported diffraction data for silver-rich chalcogenide glasses [12,40-43] and recent *ab initio* MD modelling of a $(Ag_2S)_{0.5}(As_2S_3)_{0.5}$ glass [50]. The derived DFT distances were used to plot the Haven ratio H_R of the two Ag_2S-As_2S_3 compositions. Figure 10(b) shows the Haven ratio for Ag_2S-As_2S_3, Ag_2S-GeS-GeS_2 and AgI-As_2Se_3 glasses [11,12,16] plotted as a function of $(r_{\mathrm{Ag-Ag}})^{-1}$, calculated assuming a random distribution of silver. The H_R in the critical percolation domain follows Eq. (9) while the transition to the modified-controlled region is accompanied by a step-like decrease of the Haven ratio from H_R = 0.5-0.6 to H_R = 0.3-0.4. This non-monotonic behavior was assumed to be related to a change in the silver distribution: (i) random in the critical percolation domain, and (ii) non-random in the modifier-controlled region. The Haven ratio for the 1.2 at.% Ag glass, plotted using the derived DFT distance, is located at the regression line following Eq. (9). On the contrary, the H_R for the 31.6 at.% Ag composition is shifted to higher $(r_{\mathrm{Ag-Ag}})^{-1}$, since the derived Ag-Ag separation is shorter than that for random distribution. The latter result also raises a question whether Eq. (9) has a wider applicability. In other words, the change in H_R for the modifier-controlled region would also follow Eq. (9) but this change is related to real Ag-Ag distances which can be found using structural modelling.

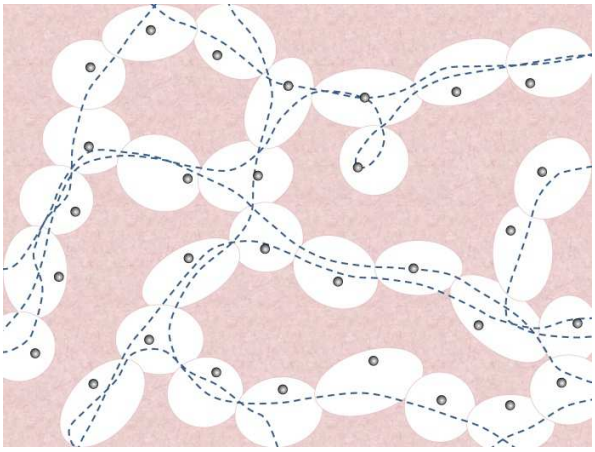

Fig. 11. Schematic representation of infinite percolation clusters in the critical percolation domain. Previously isolated allowed volumes of the glass containing mobile cations M^+ become connected at $x > x_c$ allowing the long-range diffusion. The dashed lines represent a limited number of simplified ionic migration trajectories. The majority of mobile cations are distributed randomly in the disordered network and do not have other cations as second neighbors, $\langle r_{\mathrm{M-M}} \rangle$ > 12 Å.

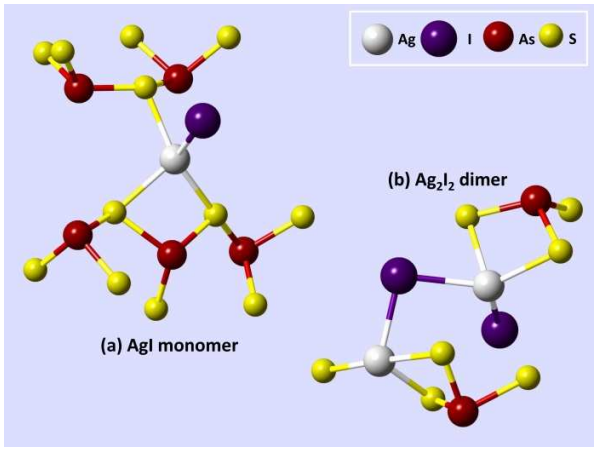

Fig. 12. Schematic representation of isolated AgY monomers or dimers in a disordered silver halide thioarsenate glass network in the critical percolation region based on initial RMC configuration of a $(AgI)_{0.2}(As_2S_3)_{0.8}$ glass.

Random silver distribution in the critical percolation domain is a key to explain the conductivity invariance of AgY- and Ag_2S-As_2S_3 glasses at $x \leq 2$ at.% Ag. The average Ag-Ag separation distance of 12 Å or more implies the absence of direct Ag-Ag contacts. It means the silver sites are isolated in a disordered glass network in the critical percolation domain as it is schematically shown in Fig. 11. When Ag^+ cation leaves the residence site and travels throughout the glass network via infinite percolation clusters, the memory of its original chemical form (sulfide or halide) vanishes rapidly with increasing the mean-square displacement. A non-random silver distribution in the modifier controlled region implying formation of preferential conduction pathways via direct contacts of edge- and corner-sharing silver chalcogenide or chalcohalide polyhedra rules out this possibility.

Preliminary RMC modelling of neutron and high-energy x-ray diffraction data for a $(AgI)_{0.2}(As_2S_3)_{0.8}$ glass also shows that the major part of silver iodide is present in the glass as isolated AgI monomers, Fig. 12. The minority species are corner-sharing Ag_2I_2 dimers. Further evolution of the structural motifs with increasing x suggests transformation of isolated oligomers into extended conduction pathways formed by connected silver chalcohalide units providing high ionic conductivity suitable for various applications. We are planning DFT and *ab initio* MD modelling of silver halide poor and rich AgY-As_2S_3 glasses to access structural details characteristic of the observed drastically different ion transport regimes.

Resuming, chemically-invariant ionic conductivity seems to be a common feature of any disordered system with random distribution of mobile ions having similar size of charge carriers. A big difference in ionic radii will affect the magnitude of $\sigma_i(x,T)$. However, recent studies of thallium thiogermanate glasses [51] show that the critical temperature T_0 remains nearly constant in comparison with silver thiogermanate vitreous alloys [11], although the difference in $\sigma_i(x)$ approaches 5 orders of magnitude between fast Ag^+ and slow Tl^+ cations. Further studies are necessary to clarify the ion size effect.

5. Conclusions

The ionic conductivity σ_i measurements of AgY-As_2S_3 (Y = Br, I) glasses, covering 13 orders of magnitude in $\sigma_i(x)$ over 5 orders of magnitude in silver content x, have shown two ion transport regimes: (i) the critical percolation at $x \leq 2$ at.% Ag, and (ii) the modifier-controlled ionic motion at x > 7-10 at.% Ag. The chemically-invariant critical percolation, characterized by a power-law dependence of $\sigma_i(x,T) \propto x^{T_0/T}$, where T_0 is the critical temperature, reveals nearly identical ionic conductivity parameters for AgY- and Ag_2S-As_2S_3 glasses. This behavior is fully reversed in the modifier-controlled region; the difference in $\sigma_i(x)$ approaches 4 orders of magnitude between AgI- and Ag_2S-As_2S_3 systems.

DFT structural modelling of two Ag_2S-As_2S_3 glasses belonging either to the critical percolation (1.2 at.% Ag) or modifier-controlled (31.6 at.% Ag) domains confirms previous structural hypothesis that silver distribution is random at low x. The observed conductivity invariance for the critical percolation is directly related to the average random Ag-Ag separation distance of 12 Å or more. When silver cation leaves its residence site and travels throughout the glass network, the memory

of its original chemical form (sulfide or halide) disappears rapidly with increasing the mean-square displacement. Chemically-invariant ionic conductivity seems to be a common feature of any disordered system with random distribution of mobile ions having similar size of charge carriers.

Corresponding authors

*Email: bychkov@univ-littoral.fr Phone: +33-328-658250.
*Email: Mohamad.Kassem@univ-littoral.fr Phone: +33-328-658270.

CRediT authorship contribution statement

The manuscript was written through contributions of all authors. All authors have given approval to the final version of the manuscript.

Declaration of Competing Interest

The authors declare no competing financial interest or personal relationships that could have appeared to influence the work reported in this paper

Acknowledgments

The authors thank the Région Hauts de France and the Ministère de l'Enseignement Supérieur et de la Recherche (CPER Climibio) as well as the European Fund for Regional Economic Development for their financial support. This work was also partly supported by the Japanese Society for the Promotion of Science under the program KAKENHI (JP16H03903). The authors are grateful to Dr. Chris J. Benmore (Argonne National Laboratory), Dr. Alex C. Hannon (ISIS Facility), Dr. Marc Fourmentin (Université du Littoral Côte d'Opale) for their help with neutron and high-energy x-ray diffraction, and SEM measurements.

References

[1] A. R. Hilton, Chalcogenide Glasses for Infrared Optics, McGraw Hill, Inc. New York, 2010.

[2] B. J. Eggleton, B. Luther-Davies, K. Richardson, Chalcogenide photonics, Nat. Photonics 5 (2011) 141–148.

[3] A. V. Kolobov, J. Tominaga , Chalcogenides: Metastability and Phase Change Phenomena, Springer, Heidelberg, 2012.

[4] J.-L. Adam, X. Zhang, eds., Chalcogenide Glasses: Preparation, Properties and Applications, Woodhead Publishing, Oxford, 2014.

[5] Y. G. Vlasov, E. A. Bychkov, Ion-selective chalcogenide glass electrodes, Ion-Selective Electrode Rev. 9 (1987) 5–91.

[6] F. Rao, K. Ding, Y. Zhou, Y. Zheng, M. Xia, S. Lv, Z. Song, S. Feng, I. Ronneberger, R. Mazzarello, W. Zhang, E. Ma, Reducing the stochasticity of crystal nucleation to enable subnanosecond memory writing, Science 358 (2017) 1423-1427.

[7] J. B. Vaney, G. Delaizir, E. Alleno, O. Rouleau, A. Piarristeguy, J. Monnier, C. Godart, M. Ribes, R. Escalier, A. Pradel, A. P. Gonçalves, E. B. Lopes, G. J. Cuello, P. Ziolkowski, E. Müller, C. Candolfi, A. Dauscher, B. Lenoir, A comprehensive study of the crystallization of Cu–As–Te glasses: microstructure and thermoelectric properties, J. Mater. Chem. A 1 (2013) 8190-8200.

[8] J. C. Bachman, S. Muy, A. Grimaud, H.-H. Chang, N. Pour, S. F. Lux, O. Paschos, F. Maglia, S. Lupart, P. Lamp, L. Giordano, Y. Shao-Horn, Inorganic solid-state electrolytes for lithium batteries: mechanisms and properties governing ion conduction, Chem. Rev. 116 (2016) 140-162.

[9] A. Hayashi, K. Noi, A. Sakuda, M. Tatsumisago, Superionic glass-ceramic electrolytes for room-temperature rechargeable sodium batteries, Nat. Commun. 3 (2012) 856.

[10] H. K. Patel, S. W. Martin, Fast ionic conduction in $Na_2S+B_2S_3$ glasses: compositional contributions to nonexponentiality in conductivity relaxation in the extreme low-alkali-metal limit, Phys. Rev. B: Condens. Matter Mater. Phys. 45 (1992) 10292-10300.

[11] E. Bychkov, V. Tsegelnik, Y. Vlasov, A. Pradel, M. Ribes, Percolation transition in Ag-doped germanium chalcogenide-based glasses: conductivity and silver diffusion results, J. Non-Cryst. Solids 208 (1996) 1–20.

[12] E. Bychkov, D. L. Price, C. J. Benmore, A. C. Hannon, Ion transport regimes in chalcogenide and chalcohalide glasses: from the host to the cation-related network connectivity, Solid State Ionics 154–155 (2002) 349–359.

[13] E. Bychkov, Superionic and ion-conducting chalcogenide glasses: transport regimes and structural features, Solid State Ionics 180 (2009) 510–516.

[14] E. Bychkov, A. Bolotov, V. Tsegelnik, Y. Grushko, Y. Vlasov, ^{64}Cu tracer diffusion in copper chalcogenide glasses, Defect Diff. Forum 194–199 (2001) 919–924.

[15] E. Bychkov, A. Bychkov, A. Pradel, M. Ribes, Percolation transition in Ag-doped chalcogenide glasses: comparison of classical percolation and dynamic structure models, Solid State Ionics 113–115 (1998) 691–695.

[16] Y. Drugov, V. Tsegelnik, A. Bolotov, Y. Vlasov, E. Bychkov, ^{110}Ag tracer diffusion study of percolation transition in $Ag_2S–As_2S_3$ glasses, Solid State Ionics 136 (2000) 1091–1096.

[17] N. F. Mott, E. A. Davis, Electronic Processes in Non-Crystalline Materials, 2nd edition, Clarendon Press, Oxford, 1979.

[18] E. Bychkov, Tracer diffusion studies of ion-conducting chalcogenide glasses, Solid State Ionics 136-137 (2000) 1111-1118.

[19] B. Roling, C. Martiny; K. Funke, Information on the absolute length scales of ion transport processes in glasses from electrical conductivity and tracer diffusion data, J. Non-Cryst. Solids 249 (1999) 201-209.

[20] S. Kirkpatrick, Percolation and conduction, Rev. Mod. Phys. 45 (1973) 574–588.
[21] S. Kirkpatrick, Models of Disordered Materials, in: R. Balian, R. Maynard, G. Toulouse (Eds.), Ill-condensed Matter, North Holland, Amsterdam, 1979: pp. 324-403.
[22] G. E. Murch, The haven ratio in fast ionic conductors, Solid State Ionics 7 (1982) 177-198.
[23] S. Hull, D. A. Keen, Pressure-induced phase transitions in AgCl, AgBr, and AgI, Phys. Rev. B: Condens. Matter Mater. Phys. 59 (1999) 750-761.
[24] E. Bychkov, D. L. Price, A. Lapp, Universal trend of the haven ratio in glasses: origin and structural evidences from neutron diffraction and small-angle neutron scattering, J. Non-Cryst. Solids 293-295 (2001) 211-219.
[25] A. Piarristeguy, M. Ramonda, N. Kuwata, A. Pradel, M. Ribes, Microstructure of Ag_2S–As_2S_3 glasses, Solid State Ionics 177 (2006) 3157–3160.
[26] T. Li, A. J. Senesi, B. Lee, Small angle X-ray scattering for nanoparticle research, Chem. Rev. 116 (2016) 11128-11180.
[27] W. Woo, M. Ohnuma, X.-L. Wang, Engineering Applications, in: F. Fernandez-Alonso, D. L. Price (Eds.), Neutron Scattering – Applications in Biology, Chemistry, and Materials Science, Academic Press, Cambridge, 2017: pp. 683-737.
[28] P. Debye, A. M. Bueche, Scattering by an inhomogeneous solid, J. Appl. Phys. 20 (1949) 518-525.
[29] P. Armand, A. Ibanez, E. Philippot, C. Williams, D. Bittencourt, Small angle X-ray scattering and the structure of Ge-S and GeS_2-Ag_2S glassy systems, J. Phys. IV Coll. 3 (1993) C8-389-C8-392.
[30] E. Bychkov, M. Miloshova, D. L. Price, C. J. Benmore, A. Lorriaux, Short, intermediate and mesoscopic range order in sulfur-rich binary glasses, J. Non-Cryst. Solids 352 (2006) 63-70.
[31] F. Fiori, F. Spinozzi, Microstructural Investigations by Small-Angle Scattering of Neutrons and X-rays, in: F. Rustichelli, J. Skrzypek (Eds.), Innovative Technological Materials: Structural Properties by Neutron Scattering, Synchrotron Radiation and Modeling, Springer, Heidelberg, 2010: pp. 35-78.
[32] T. Usuki, S. Saito, K. Nakajima, O. Uemura, Y. Kameda, T. Kamiyama, M. Sakurai, Structural and electrical properties of AgI dispersed As-chalcogenide glasses, J. Non-Cryst. Solids 312–314 (2002) 570–574.
[33] Y. Onodera, T. Furukawa, S. Hashimoto, T. Usuki, Y. Amo, Y. Kameda, Vitrification and transport properties in AgBr-doped chalcogenide systems, Solid State Ionics 177 (2006) 2597–2599.
[34] I. Alekseev, M. Kassem, M. Fourmentin, D. Le Coq, R. Iizawa, T. Usuki, E. Bychkov, Ionic and electronic transport in AgI–As_2Te_3 glasses, Solid State Ionics 253 (2013) 181–184.
[35] Y. M. Ben-Shaban, Ion transport in AgY-Sb_2S_3 (Y = Cl, Br, I) glasses, Doctoral dissertation, St. Petersburg University, St. Petersburg, Russia, 1997.
[36] Yu. G. Vlasov, E. A. Bychkov, B. L. Seleznev, Compositional dependence of ionic conductivity and diffusion in mixed chalcogen Ag-containing glasses, Solid State Ionics 24 (1987) 179–187.
[37] E. Soignard, O. B. Tsiok, A. S. Tverjanovich, A. Bytchkov, A. Sokolov, V. V. Brazhkin, C. J. Benmore, E. Bychkov, Pressure-driven chemical disorder in glassy As_2S_3 up to 14.7 GPa, postdensification effects, and applications in materials design, J. Phys. Chem. B 124 (2020) 430–442.
[38] A. Tverjanovich, M. Khomenko, C. J. Benmore, S. Bereznev, A. Sokolov, D. Fontanari, A. Kiselev, A. Lotin, E. Bychkov, Atypical phase-change alloy Ga_2Te_3: atomic structure, incipient nanotectonic nuclei, and multilevel writing, J. Mater. Chem. C 9 (2021) 17019–17032.
[39] R. Zaiter, Silver and/or mercury doped thioarsenate and thiogermanate glasses: Transport, structure and ionic sensibility, Ph.D. thesis, Université du Littoral Côte d'Opale, 2018.
[40] I. T. Penfold, P. S. Salmon, Glass formation and short-range order in chalcogenide materials: the $(Ag_2S)_x(As_2S_3)_{1-x}$ ($0 \le x \le 1$) pseudobinary tie line, Phys. Rev. Lett. 64 (1990) 2164-2167.
[41] J. H. Lee, A. P. Owens, A. Pradel, A. C. Hannon, M. Ribes, S. R. Elliott, Structure determination of Ag-Ge-S glasses using neutron diffraction, Phys. Rev. B: Condens. Matter Mater. Phys. 54 (1996) 3895-3909.

[42] E. Bychkov, D. L. Price, Neutron diffraction studies of Ag_2S–As_2S_3 glasses in the percolation and modifier-controlled domains, Solid State Ionics 136–137 (2000) 1041–1048.
[43] Y. Onodera, T. Usuki, T. Nasu, S. Kohara, Structure of silver bromide doped chalcogenide glasses, Solid State Ionics 262 (2014) 469-471.
[44] G. N. Greaves, EXAFS and the structure of glass, J. Non-Cryst. Solids 71 (1985) 203-217.
[45] S. Adams, J. Swenson, Determining ionic conductivity from structural models of fast ionic conductors, Phys. Rev. Lett. 84 (2000) 4144-4147.
[46] C. Escher, T. Latychevskaia, H.-W. Fink, D. W. Pohl, Direct evidence for conduction pathways in a solid electrolyte, Phys. Rev. Lett. 97 (2006) 136601.
[47] S. Adams, R. P. Rao, Transport pathways for mobile ions in disordered solids from the analysis of energy-scaled bond-valence mismatch landscapes, Phys. Chem. Chem. Phys. 11 (2009) 3210-3216.
[48] K. Mori, T. Ichida, K. Iwase, T.Otomo, S. Kohara, H. Arai, Y. Uchimoto, Z. Ogumi, Y. Onodera, T. Fukunaga, Visualization of conduction pathways in lithium superionic conductors: Li_2S-P_2S_5 glasses and $Li_7P_3S_{11}$ glass–ceramic, Chem. Phys. Lett. 584 (2013) 113–118.
[49] M. Marple, D. C. Kaseman, S. Kim, S. Sen, Superionic conduction of silver in homogeneous chalcogenide glasses, J. Mater. Chem. A 4 (2016) 861–868.
[50] J. Akola, P. Jóvári, I. Kaban, I. Voleská, J. Kolář, T. Wágner, R. O. Jones, Structure, electronic, and vibrational properties of amorphous AsS_2 and $AgAsS_2$: experimentally constrained density functional study, Phys. Rev. B: Condens. Matter Mater. Phys. 89 (2014) 064202.
[51] M. Bokova, I. Alekseev, D. Kalyagin, V. Tsegelnik, Y. Ermolenko, E. Bychkov, ^{204}Tl tracer diffusion and conductivity in thallium thiogermanate glasses, Solid State Ionics 253 (2013) 101-109.